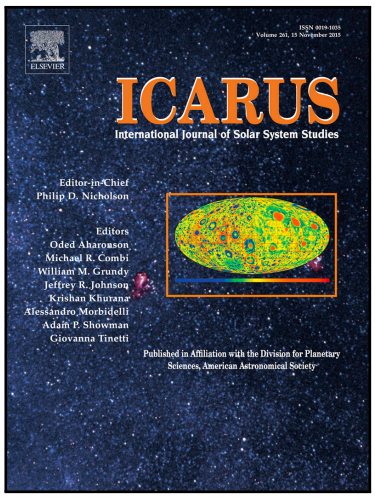

Analysis of gaseous ammonia (NH_3) absorption in the visible spectrum of Jupiter

Patrick G.J. Irwin, Neil Bowles, Ashwin S. Braude, Ryan Garland, Simon Calcutt

PII: S0019-1035(17)30547-X
DOI: 10.1016/j.icarus.2017.11.031
Reference: YICAR 12715

To appear in: *Icarus*

Received date: 27 July 2017
Revised date: 24 October 2017
Accepted date: 27 November 2017

Please cite this article as: Patrick G.J. Irwin, Neil Bowles, Ashwin S. Braude, Ryan Garland, Simon Calcutt, Analysis of gaseous ammonia (NH_3) absorption in the visible spectrum of Jupiter, *Icarus* (2017), doi: 10.1016/j.icarus.2017.11.031

Highlights

- Available sources of ammonia absorption in visible/near-IR compared and analysed
- Band data of Bowles et al. (2008) found to combine best accuracy and coverage
- Find absence of reliable absorption data below 0.758 μm under Jovian conditions
- Findings relevant to solar system and future vis/NIR observations of cool planets

Analysis of gaseous ammonia (NH_3) absorption in the visible spectrum of Jupiter

Patrick G. J. Irwin, Neil Bowles, Ashwin S. Braude, Ryan Garland, and Simon Calcutt

Department of Physics, University of Oxford, Parks Rd, Oxford OX1 3PU, UK.

patrick.irwin@physics.ox.ac.uk

Received _____; accepted _____

Submitted to Icarus.

ABSTRACT

Observations of the visible/near-infrared reflectance spectrum of Jupiter have been made with the Very Large Telescope (VLT) Multi Unit Spectroscopic Explorer (MUSE) instrument in the spectral range 0.48 – 0.93 μm in support of the NASA/Juno mission. These spectra contain spectral signatures of gaseous ammonia (NH_3), whose abundance above the cloud tops can be determined if we have reliable information on its absorption spectrum. While there are a number of sources of NH_3 absorption data in this spectral range, they cover small sub-ranges, which do not necessarily overlap and have been determined from a variety of sources. There is thus considerable uncertainty regarding the consistency of these different sources when modelling the reflectance of the entire visible/near-IR range. In this paper we analyse the VLT/MUSE observations of Jupiter to determine which sources of ammonia absorption data are most reliable. We find that the band model coefficients of Bowles et al. (2008) provide, in general, the best combination of reliability and wavelength coverage over the MUSE range. These band data appear consistent with ExoMOL ammonia line data of Yurchenko et al. (2011), at wavelengths where they overlap, but these latter data do not cover the ammonia absorption bands at 0.79 and 0.765 μm, which are prominent in our MUSE observations. However, we find the band data of Bowles et al. (2008) are not reliable at wavelengths less than 0.758 μm. At shorter wavelengths we find the laboratory observations of Lutz and Owen (1980) provide a good indication of the position and shape of the ammonia absorptions near 0.552 μm and 0.648 μm, but their absorption strengths appear inconsistent with the band data of Bowles et al. (2008) at longer wavelengths. Finally, we find that the line data of the 0.648 μm absorption band of Giver et al. (1975) are not suitable for modelling these data as they account for only 17% of

the band absorption and cannot be extended reliably to the cold temperatures and H_2/He-broadening conditions found in Jupiter's atmosphere. This work is of significance not only for solar system planetary physics, but also for future proposed observations of Jupiter-like planets orbiting other stars, such as with NASA's planned Wide-Field Infrared Survey Telescope (WFIRST).

Subject headings: Jupiter, atmosphere; Saturn, atmosphere; Extra-solar planets; Radiative transfer; Spectroscopy

1. Introduction

In support of the NASA/Juno mission (Matousek 2007) we have recently observed Jupiter with the MUSE (Multi Unit Spectroscopic Explorer, Bacon et al. (2010)) instrument at ESO's (European Southern Observatory) Very Large Telescope (VLT). MUSE records complete visible/near-infrared spectra (0.48 – 0.93 μm) from all points on Jupiter's observable disc. These observations will be used to track the development of cloud structures and study the distribution of colour-carrying particles, or 'chromophores'. These data also contain a number of absorption features of ammonia gas at 0.55 μm, 0.65 μm, and further bands increasing in strength between 0.74 μm and 1 μm. Given reliable information on the strength of these bands, we may use these features to determine the abundance of ammonia above the cloud tops. However, available ammonia absorption data come from a range of sources whose consistency with respect to each other has not been properly tested against observational data. This is of importance not only to studies of Jupiter's atmosphere, but also to future study of Jupiter-like exoplanets, whose reflectivity spectra could potentially be determined with coronographic direct-imaging using space telescopes such as NASA's planned Wide-Field Infrared Survey Telescope (WFIRST) (e.g. Spergel et al. 2013). In this paper we review the available sources of visible/near-IR gaseous ammonia absorption data and assess their validity and consistency between these data sets.

2. Spectral Data Sources

There appear to be four main sources of gaseous ammonia absorption data in the visible/near-infrared region. The data reported by Giver et al. (1975), Lutz and Owen (1980) and Bowles et al. (2008) come from measuring the absorption of ammonia gas in laboratory paths at medium or high resolution, and fitting either mean absorption coefficients, (Lutz and Owen 1980), band models (Bowles et al. 2008), or line strengths

for a selection of the strongest lines (Giver et al. 1975). The band data of Bowles et al. (2008) were observed at temperatures between 220 and 292K, but the data of Giver et al. (1975) and Lutz and Owen (1980) are limited to room temperature only and thus it is difficult to know how best to extrapolate these observations to the colder temperatures in Jupiter's atmosphere. In addition, all three laboratory measurement studies were measured under self-broadening conditions only, rather than H_2/He-broadening as experienced in Jupiter's atmosphere. Hence, there is also uncertainty in how to correct these observations for foreign-broadening conditions. The 5520Å (i.e. 0.552 μm) band is reported only by Lutz and Owen (1980), while the 6475Å (i.e. 0.6475 μm) band is reported by both Lutz and Owen (1980) and Giver et al. (1975). The laboratory data of Bowles et al. (2008) covers wavelengths longer than 0.74 μm, in the form of band model coefficients, which are temperature dependent. More recently the ExoMOL project has computed an *ab initio* line table for NH_3 from first principles (Yurchenko et al. 2011). These data cover wavelengths longer than 0.833 μm, but only include line strengths and lower state energies and do not have any information on line widths. Hence, further analysis and assumptions have to be made to assign line widths (under H_2/He-broadening conditions) and their temperature dependences in order to apply these data to radiative transfer calculations under Jovian conditions.

These different gaseous ammonia absorption data sources are reviewed individually and in more detail below.

2.1. ExoMOL NH_3

The ExoMOL *ab initio* ammonia line table of Yurchenko et al. (2011) includes line strengths and lower state energies and lists over 1 billion lines in the spectral range 0 – 12000 cm^{-1} (i.e. wavelengths longer than 0.833 μm). Most of the lines are 'hot lines' that

only become important at high temperature (i.e. $T > 400$ K) and are not important at Jovian temperatures.

The strength of a line at temperature T, $S(T)$, compared with that observed at the reference temperature T_0 (taken to be 296 K), $S(T_0)$, may be calculated from the equation:

$$\frac{S(T)}{S(T_0)} = \frac{Q_V(T_0)Q_R(T_0)(1-\exp(-E_T/kT))\exp(-E_l/kT)}{Q_V(T)Q_R(T)(1-\exp(-E_T/kT_0))\exp(-E_l/kT_0)} \quad (1)$$

where $Q_V(T)$ and $Q_R(T)$ are the vibration and rotation partition functions, respectively, $(1-\exp(-E_T/kT))$ is a correction for stimulated emission, equal to one minus the ratio of Boltzmann populations for the two states (E_T is the transition energy), and $\exp(-E_l/kT)$ is the Boltzmann population of the lower state, of energy E_l.

Figure 1 demonstrates, using Eq. 1, how the line strength correction, $S(T)/S(T_0)$, is expected to vary with temperature for lines near 6475Å with different lower energies (LSE). It can be seen that lines with higher lower state energies quickly diminish in strength as the temperature is reduced, while the stimulated emission term is negligible at these wavelengths. It can also be seen that the total partition function provided by HITRAN2012 (Rothman et al. 2013) is well approximated by just the expected rotational component for a polyatomic molecule of $(T_0/T)^{3/2}$.

Since the ExoMOL line database lists many lines that are not relevant for calculating ammonia opacities in Jupiter's atmosphere, we initially reduced the number of lines to a more manageable level by using the lower state energies and partition function to compute the line strengths at 400 K and neglected lines contributing less than 10^{-4} % to the total line strength (summed over 1 cm^{-1}-wide bins). Once we had reduced the number of lines, we then needed to add line-broadening information since (unless the lines are to be used for calculations at low pressure and high temperature, where only Doppler-broadening of the lines is important) we need information on the pressure-broadened line widths to compute the Voigt lineshape for each line. Following Amundsen et al. (2014) and Garland and

Irwin (2017), the foreign broadening line widths of the NH_3 lines in a solar composition H_2-He atmosphere (assumed by Garland and Irwin (2017) to be 85:15, very similar to the Jovian value used in analysing our Cassini/CIRS observations from Irwin et al. (2004) of 0.865:0.135) were allocated (depending on the rotational energy level J) from the data of Pine et al. (1993). The temperature dependence exponents of these widths were taken from Nouri et al. (2004) and Sharp and Burrows (2007) for H_2-broadening and He-broadening, respectively, and used to compute a weighted-average of 0.66 (Garland and Irwin 2017). To compare with laboratory measurements under self-broadening conditions, self-broadened line widths were also taken from Pine et al. (1993), while the temperature dependence exponent was set to the default expected theoretical value of 0.5. The ExoMOL linedata with these modifications were then used to compute k-distribution look-up tables for both H_2-He- and self-broadening conditions, covering the spectral range 0.4 – 1.0 μm. These k-tables are used in our correlated-k radiative transfer model, NEMESIS, described later. In these k-tables, 10 g-ordinates were used with 15 pressures logarithmically spaced between 10^{-4} and 10 bar and 20 temperatures equally spaced between 50 and 400K. It should be noted that we had to convert the ExoMOL line data to k-tables (and use a correlated-k, rather than a line-by-line model), since our other sources of ammonia absorption are either in the form of band data or average absorption coefficients. In addition, our best source for methane absorption, which is the dominant gaseous absorption seen in Jupiter's visible – near-IR spectrum (Karkoschka and Tomasko 2010) is also in the form of band data, to which we fitted k-coefficients using exponential-sum fitting.

2.2. Lutz and Owen (1980) absorption data

Lutz and Owen (1980) report room temperature laboratory measurements of the absorption spectrum of NH_3 for both the 6475 Å band and the 5520 Å band at a spectral

resolution of 2Å. Their estimate of the total band intensity is 0.63 cm^{-1} (m-amagat)$^{-1}$ at 6475 Å (in good agreement with Giver et al. (1975)) and 0.096 cm^{-1} (m-amagat)$^{-1}$ for the much weaker 5520 Å band. These data are presented in the form of apparent absorption cross-sections, but as their data do not resolve individual lines, they cannot strictly be used as monochromatic absorption data. Hence, Lutz and Owen (1980), give 'curve-of-growth' tables that allow their band-integrated absorptions (or equivalent widths) to be scaled appropriately as individual lines within the bands become saturated depending on the total path length of ammonia between the cloud top and the observer. The authors note that under Jovian conditions the 5520Å band is always in the weak limit and thus the equivalent width increases linearly with the path abundance, but they state that the 6475Å band can slightly saturate. However, they give no method for calculating how the shape of the absorption spectrum changes, and their 'curve-of-growth' method relies on calculating the total path length between the cloud tops and the observer and making a correction for the band-integrated absorption. While such a method is of use for reflecting layer model calculations, it is not possible to apply the same technique for multiple-scattering calculations, where the transmission of the various scattering layers are multiplied. To account for temperature variations, Lutz and Owen (1980) suggest a simple temperature scaling of the form $W = W_0(T/T_0)^{1/2}$, where W is the band-integrated strength. Such a scaling is suitable for line widths, but it is not clear how suitable this is for line strengths. However, from Fig,1 we can see that such a temperature dependence is broadly similar to the line strength variation we might expect for lines with lower state energies of ~ 300 cm^{-1}, typical of lines at longer wavelengths in the visible/near-infrared region, as we shall see later.

2.3. Giver (1975) absorption data

Giver et al. (1975) present high-resolution (R= $\lambda/\Delta\lambda = 170,000$) laboratory spectra of self-broadened ammonia in the 6475 Å band at room temperature, and also report the line strengths of the strongest lines observed. These were compiled into a line data table, using a mean H_2-broadened linewidth for all lines of 0.101 cm^{-1}, which is an average of the H_2-broadened linewidths of lines in this band reported by Keffer et al. (1985, 1986), and using the self-broadened line widths quoted for each line by Giver et al. (1975) directly. However, a key drawback of these data is that they pertain only to room temperature observations and do not include an estimate of the lower state energy. Without such an estimate it is difficult to use these data to model the infrared spectrum of a cold planet such as Jupiter since we cannot compute how the strengths vary with temperature. In addition, these data only include the very strongest of lines and thus when used to simulate low-resolution spectra completely fail to account for the large number of weak lines that are present and which add up to provide most of the absorption. This can be seen in Fig. 2, which reproduces the observed 'low-dispersion' transmission spectrum of a 36-m path of self-broadened ammonia at 294K and 1.0 atm, shown in Fig.3 of Giver et al. (1975). Unfortunately, the spectral resolving power of this 'low-dispersion' spectrum is not quoted by Giver et al. (1975). Also shown on Fig. 2 are the transmission spectrum calculated with the Lutz and Owen (1980) absorption data, and with the Giver et al. (1975) line data, both at high resolution and also smoothed to a resolution of 2 Å to allow direct comparison with the calculated spectrum using the Lutz and Owen (1980) absorption data. We find that the data of Lutz and Owen (1980) reproduce the overall transmission of the observed spectrum very well, albeit at lower resolution. However, we can see in Fig. 2 that the absorption calculated with the line data of Giver et al. (1975) is significantly underestimated. This discrepancy is easily understood since when the published line strengths of Giver et al. (1975) are added, the total band intensity is found to be 0.11 cm^{-1}

(m-amagat)$^{-1}$, which is much less than the authors' own estimate from the low-dispersion spectrum of 0.66 cm^{-1} (m-amagat)$^{-1}$, accounting for only 17% of the band-integrated absorption. Hence, while of interest, the line data of Giver et al. (1975) in the 6475 Å band are not useful in modelling moderate-resolution spectroscopic observations of Jovian planets as they do not account for all the lines in the band, and do not include lower state energies necessary to extrapolate the line strengths to lower temperatures.

2.4. Bowles et al. (2008) band data

Bowles et al. (2008) report band models fitted to the measured absorption spectra of laboratory paths of ammonia with path lengths of 2.164 and 10.164 m, pressures ranging from 0.075 to 1.02 bar and temperatures varying between 216 and 292 K. The measured transmission spectra cover the spectral range 0.74 - 1.0475 μm and have a spectral resolution and step of 0.0025 μm. These transmission spectra were fitted with a Goody-Lorentz model (Goody 1952), which calculates the transmission τ of a path with absorber amount U (molecule cm^{-2}), pressure p, temperature T to be

$$\tau = \exp\left(-1/\sqrt{\frac{1}{\left(k_\nu(T)U\right)^2} + \frac{1}{\pi k_\nu(T) y_\nu U p \sqrt{\frac{T_0}{T}}}}\right) \tag{2}$$

where the mean absorption strength at temperature T, $k_\nu(T)$, is calculated as

$$k_\nu(T) = k_\nu(T_0)\left(\frac{T_0}{T}\right)^{1.5} \exp\left[1.439 E_{\nu l}\left(\frac{1}{T_0} - \frac{1}{T}\right)\right]. \tag{3}$$

The fitted parameters of this model are the absorption strength at reference temperature T_0, $k_\nu(T_0)$, the mean lower state energy, $E_{\nu l}$, and an effective line width parameter, y_ν, where ν is the wavenumber or wavelength and the reference temperature $T_0 = 296$ K. The

main temperature dependance of this model is clearly very similar to that assumed for line-by-line (LBL) models, but the fitted parameters are not constrained to be limited to physically plausible values. This can be seen in Fig. 3 where we compare the tabulated values of $k_\nu(T_0)$, $E_{\nu l}$ and y_ν with equivalent values extracted from the ExoMOL NH_3 database (Yurchenko et al. 2011), i.e. the line strengths at T_0, the strength-weighted lower state energies and strength-weighted self-broadening line-widths of Pine et al. (1993), all themselves averaged over bins of width and step 0.0025 μm as used by Bowles et al. (2008).

As can be seen in Fig.3, the ExoMOL data of Yurchenko et al. (2011) and the band data of Bowles et al. (2008) are remarkably consistent at wavelengths where they overlap. The data of Bowles et al. (2008) uniquely cover the 0.74 to 0.833 μm region, but become increasingly noisy at shorter wavelengths. The shortest wavelength absorptions were only visible at the longest path lengths, highest pressures and highest temperatures in the laboratory measurements and these features were essentially lost in the noise at lower temperatures. This is because at lower temperatures, since the pressure cannot be allowed to exceed the saturated vapour pressure of ammonia (to avoid condensation on the surfaces of the experiment) this necessarily limits the path absorber amounts, U, that can be attained. Hence, the strengths become increasingly 'noisy' and the fitted values of E_l and y_ν increasingly scattered, which makes the extrapolated absorptions at lower temperatures less reliable, although in general, the lower state energies E_l seem to have a value of roughly 300 cm^{-1} in this wavelength region. Figure 4 shows the laboratory spectra measured by Bowles et al. (2008) at the longest available path absorber amounts, U, for four temperatures in the range 215 – 295 K. Here we can see that, while there appear to be consistent observations of the stronger absorption bands at wavelengths longer than 0.775 μm, the data for the bands at shorter wavelengths are obscured by noise. Hence, these transmission data do not contain enough information to meaningfully constrain the $k_\nu(T_0)$, $E_{\nu l}$ and y_ν parameters and so the band data must be used with caution at these

wavelengths, especially at lower temperatures, as we shall see later.

Although measured under self-broadening conditions, Bowles et al. (2008) made these data more useful for Jovian planet modelling by giving a 'self-to-foreign-broadening' ratio, SFB = 5, which converts the y_ν parameter, estimated here for self-broadening conditions, to values appropriate for foreign-broadening conditions of y_ν/SFB. This assumption of the ratio between self- and hydrogen/helium-broadening of ammonia lines is in generally good agreement with the laboratory measurements of individual lines reported by Keffer et al. (1986), Pine et al. (1993), and Giver et al. (1975).

These band data were used to compute k-tables with the same parameters as used to generate k-tables from the ExoMOL data, using the method of 'exponential sum fitting', as described by Irwin et al. (1999). These tables were calculated for both self-broadening and H_2/He-broadening conditions, using for the latter the estimated self-to-foreign-broadening ratio, SFB = 5.

3. MUSE observations

The Multi Unit Spectroscopic Explorer (MUSE) instrument at ESO's Very Large Telescope in Chile is an Integral-field Spectrograph, which records 300 × 300 pixel images from a field of view of 60″× 60″ (in wide field mode), but where each 0.2″ × 0.2″ pixel contains a complete visible/near-infrared spectrum (0.48 – 0.93 μm) with a spectral resolving power of 2000 – 4000 (i.e. a spectral resolution of 2.3Å). The observations of Jupiter recorded by MUSE have reasonably good spatial resolution due to the generally excellent "seeing" at the location of VLT, of typically $< 0.8''$. This can be seen in Fig. 5, which shows a typical observation recorded on March 8th 2016, displayed as 'true-colour' and false-colour images, showing the Great Red Spot (GRS) at lower left. The MUSE

observations are made up of a set of nine exposures, seven of Jupiter and two of sky, of just 0.1s exposure time each, but with 2 minutes required to read out each frame.

In contrast to the MUSE spectral resolution of 2.3Å, the best available source of methane absorption in this spectral range are the band model coefficients of Karkoschka and Tomasko (2010), to which we have fitted k-distributions, using exponential-sum fitting. These data have a spectral resolution of 25 cm^{-1} between 19300 and 25000 cm^{-1} (0.518 - 0.4 μm), and 10 cm^{-1} at wavenumbers less than 19300 cm^{-1} (0.518 μm). These resolutions equate to roughly 5 Å (i.e. 0.0005 μm) across the visible range and so the MUSE data cannot be analysed using these coefficients at their native resolution. Hence, the data were first smoothed to make them more compatible with the available sources of methane and ammonia data. Given the spectral resolution of the available absorption data sources (especially for ammonia) we smoothed the MUSE spectra to the resolution of the IRTF/SpeX instrument, which has a triangular instrument function with FWHM = 2 nm (i.e 0.002 μm), sampled at 0.001 μm. We constructed our k-tables to have this same resolution.

The MUSE data were reduced with the VLT/MUSE standard pipeline (Ballester et al. 2006) and photometrically calibrated with an observatory-selected white dwarf star. To check this calibration, Fig. 6 compares the integrated disc-averaged MUSE reflectance spectrum observed on 28th May 2017 with the albedo spectrum of Karkoschka (1994), showing the generally good agreement, to within 10% at worst. Since the data observed by Karkoschka (1994) were measured in 1993, it is not surprising that there are some differences compared with the current state of a planet with such highly active and changing clouds as Jupiter. For this reflectance calculation, the observed radiances were divided by a reference solar spectrum, using Jupiter's distance from the sun of 5.45AU on this date. For this, the solar spectrum of Chance and Kurucz (2010) was used, which was

first smoothed with a triangular line shape of FWHM = 0.002 μm to make it compatible with our smoothed spectra. We found this solar spectrum to be more reliable at shorter wavelengths than that of Thuillier et al. (2003), sometimes used in this wavelength region.

4. Analysis of MUSE observations

Figure 7 shows two typical spectra extracted from the MUSE data from 28th May 2017, one averaged over a 11 × 11-pixel box in the Equatorial Zone (mean latitude 0.65°S, range ∼ 3.65°S – 2.35°N) near the sub-Earth point and another averaged over a 9 × 9-pixel box in the North Equatorial belt (mean latitude 12.4°N, range ∼ 9.9°N – 14.9°N), near the central meridian. These spectra were modelled with our NEMESIS (Irwin et al. 2008) radiative transfer and retrieval tool. This model uses the method of correlated-k (e.g. Lacis and Oinas (1991)) in its radiative transfer scheme, and combines the k-distribution tables of different gases using the overlapping line approximation (Lacis and Oinas 1991). To model the multiple-scattering conditions of reflected sunlight in Jupiter's atmosphere, NEMESIS uses the matrix-operator method of Plass et al. (1973). This model uses Gauss-Lobatto quadrature to integrate the upwelling and downwelling radiance fields over zenith angle, using a 5-zenith-angle quadrature scheme in this case. The azimuth part of the integration is achieved with Fourier decomposition, and the number of components, n, for this was set by the minimum of the reflected (θ°_{ref}) or incident-solar (θ°_{inc}) zenith angles as $n = mod(min(\theta_{inc}, \theta_{ref})/3)$. The absorption of ammonia gas at wavelengths longer than 0.74 μm was modelled here with the band data of Bowles et al. (2008), converted to k-tables as previously described, while ammonia absorption at 0.55 and 0.65 μm was directly modelled using the apparent cross-sections of Lutz and Owen (1980), with no temperature dependance assumed. Methane absorption was modelled with a k-table generated from the band data of Karkoschka and Tomasko (2010), while small

absorption features from H_2 lines were modelled with a k-table generated from line data from the HITRAN2012 line database (Rothman et al. 2013). The collision-induced absorption of H_2-H_2 at these wavelengths was modelled after Zheng and Borysow (1995), while at shorter wavelengths, the Rayleigh-scattering opacity was modelled via standard theory (e.g. Goody and Yung (1989)), accounting for the contributions of H_2, He, CH_4 and NH_3. To model these observations, a 'standard' Jupiter atmosphere was constructed with deep mole fractions of H_2, He, CH_4 and NH_3 set to 0.8622, 0.1339, 1.81×10^{-3} and 2×10^{-4}, respectively, with the abundance of NH_3 limited to the saturated vapour mole fraction at lower temperatures. This atmospheric profile is the same as was used to model Cassini/CIRS observations of Jupiter (Irwin et al. 2004). To understand how these gas opacities and Rayleigh-scattering opacities affect the reflectivity spectrum of Jupiter's atmosphere, Fig. 8 shows the transmission to and from successively deeper pressure levels in our assumed Jupiter atmosphere for cloud-free conditions. The increasing importance of Rayleigh scattering can be seen at shorter wavelengths, but at most wavelengths the Jovian air is relatively clear, with the main absorption features arising from methane, especially near 0.72 μm, where we see we are really only sensitive to reflection from particles at pressures less than 300 mb, and near 0.89 μm, where we can only detect the reflection from particles lying at pressures less than 100 – 200 mb.

For our scattering calculations, the atmosphere was split up into 39 levels equally spaced in log(pressure) between 10 and 10^{-4} bar. Clouds/hazes in the atmosphere were modelled with a continuous distribution of aerosols whose *a priori* abundance (opacity/mass) was set to 0.01 (g cm^{-2})$^{-1}$, where our opacities refer to that observed at a wavelength of 0.6 μm. The scattering properties of these aerosols were calculated using the method of Irwin et al. (2015), which uses Mie theory, assuming a fixed size distribution of particles (standard gamma after Hansen (1971)) with mean radius 1.0 μm and variance 0.05, a fixed real refractive index at 0.6 μm of 1.4 (similar to ammonia ice) and a variable imaginary

refractive index spectrum of the particles, computing the real part of the complex refractive index using the Kramers-Kronig method (e.g. Sheik-Bahae 2005). The spectra were modelled by fitting the vertical profile of aerosol abundance, fitting the imaginary refractive index spectrum of the particles and multiplying the *a priori* ammonia abundance by a simple scaling factor. The results of this retrieval model applied to the reference EZ and NEB spectra can be seen in Fig. 7. In these retrievals we found that we were unable to fit the MUSE spectra to within the random errors estimated from the reduction pipeline, which we attribute to deficiencies and uncertainties in our gaseous absorption coefficients and other assumptions made in our forward modelling. Hence an additional 'forward modelling' error of 5×10^{-5} W cm^{-2} sr^{-1} μm^{-1} was added to the spectra at all wavelengths, which allowed us to fit the spectra to a precision $\chi^2/n \sim 1$, and gives more realistic error limits on our retrieved parameters. This treatment of forward modelling uncertainties is routine in the optimal estimation approach adopted by NEMESIS in conditions such as this, where the data are measured to a better precision than can be modelled with existing sources of absorption/scattering coefficients. In Fig. 7 we can see that the spectra for both locations are well modelled with a cloud with peak abundance near the 1-bar level. Our retrieved imaginary refractive indices show significant blue absorption in both spectra, with generally increased absorption across all wavelengths in the NEB relative to the EZ. In both locations we found that an ammonia abundance less than that initially assumed gives the best fit, with ammonia more depleted in the NEB than the EZ, which is consistent with other measurements of the distribution of ammonia in Jupiter's atmosphere. It should be noted that for both regions we thus find ammonia to be sub-saturated above the clouds. Although we used a simple scaled ammonia profile for these fits, we tested our vertical sensitivity to ammonia, by perturbing the abundance of ammonia in this profile at different levels and calculating the change in radiance. As we are seeing absorption from ammonia in and above the clouds our vertical sensitivity to this gas is defined by pressure levels where

the cloud opacity is not too high to limit the sunlight, but where the ammonia abundance (which drops rapidly with height) is still significant, i.e. immediately above the cloud tops. Our retrieved cloud profile has maximum opacity at 1 bar, and we found that our sensitivity to ammonia also peaks at this level. The inferred cloud absorption spectrum of the cloud particles is similar to that of a material generated in the laboratory by reacting photodissociated ammonia with acetylene (C_2H_2), reported by Carlson et al. (2016) and used by Sromovsky et al. (2017) to model Cassini/VIMS observations of Jupiter, recorded in 2000, covering the spectral range 0.3 to 1.05 μm.

We are clearly able to fit the VLT/MUSE observations of the EZ and NEB very well with this model, but there are some significant differences. These can be seen more clearly in Fig. 9 for the EZ and Fig. 10 for the NEB, where we have also shown the spectra modelled without the ammonia data of Bowles et al. (2008) and Lutz and Owen (1980), and then with the absorption of ammonia at wavelengths $> 0.7\mu$m, modelled instead with ExoMOL (Yurchenko et al. 2011). Key 'visible' ammonia absorption features are marked in Figs. 9 and 10 as: A – 0.552 μm, B – 0.648 μm, C – 0.75 μm, D – 0.76 μm, E – 0.79 μm, F – 0.825 μm and G – 0.93 μm.

First of all, we find that for the wavelengths covered by both band data and line data (i.e. at $\lambda > 0.833$ μm) the difference between the spectra calculated with the band data of Bowles et al. (2008) and the ExoMOL line data of Yurchenko et al. (2011) are very small, although the ExoMOL line data perhaps slightly better model absorption feature G (0.93 μm). Moving to wavelengths shorter than 0.833 μm, we can see that the band data of Bowles et al. (2008) fit feature E (0.79 μm) well, and to a lesser extent feature F (0.825 μm). Since most of the reflection comes from clouds near 1 bar, the mass-weighted mean temperature of the path above the clouds to space is $\sim$ 138 K, which is well beyond the range of temperatures measured by Bowles et al. (2008), and it is a testament to

the careful measurements and reliability of the Goody-Lorentz band model that the data can predict the spectra so well for features E – G. However, as we might expect from our analysis of the laboratory measurements earlier, we find that the band data of Bowles et al. (2008) provides a less good fit to feature D at 0.76 μm (predicting too little absorption), and predicts a feature to be present at 0.75 μm, which is absent from the observed Jovian spectra. Hence, we conclude that the band data of Bowles et al. (2008) are not reliable at wavelengths $\lambda < 0.758$ μm. At shorter wavelengths, we find that while the features A (0.552 μm) and B (0.648 μm) are predicted to be visible in the modelled spectra using the coefficients of Lutz and Owen (1980), they do not have quite enough absorption at 0.648 μm, and have clearly insufficient absorption at 0.552 μm. When using these coefficients, we did not use the temperature dependence suggested by Lutz and Owen (1980), which would have reduced the absorption strength still further for a mean path temperature of $\sim$ 138 K, but at the same time we used the data as a continuum absorption, which is not strictly applicable for a feature that is actually composed of thousands of thin lines. It might be possible to take these data and use the 'curve-of-growth' tables of Lutz and Owen (1980) to compute transmission spectra for a range of path lengths and fit k-distributions to these synthetic transmittances using exponential-sum fitting. However, the 'curve-of-growth' tables give no indication of how the shape of the absorption features might change with path length and we would still have no reliable information on their temperature dependance. We could conceivably introduce some temperature dependence by assuming that these bands can be modelled with a Goody-Lorentz model (as Bowles et al. (2008)), and set the lower state energy $E_{l\nu}$ and broadening y_ν parameters to values consistent with that found at longer wavelengths, but we concluded that this would involve just too many assumptions. Also, we have found that these data, even as measured at room temperature, do not appear to give sufficient absorption to be consistent with the longer-wavelength absorption data of Bowles et al. (2008) and Yurchenko et al. (2011). Hence, while these data may provide a

useful tool for analysing spectra that just cover the 0.5 – 0.7 μm spectral range, we conclude that they are too inconsistent with absorption data at longer wavelengths (i.e. Bowles et al. (2008), Yurchenko et al. (2011)) to allow them to be used reliably in fits to this entire spectral range.

Aside from the ammonia features, just described, there are other differences between the estimated and modelled reflectance spectra, which could arise from a number of causes. Firstly, to calculate the reflectivity we need to divide the measured radiance spectrum by that of sunlight reflected from a Lambertian surface at the same distance from the Sun at normal incidence to it, i.e. I/F = $R/(\pi F)$, where R is the observed spectral radiance (W cm^{-2} sr^{-1} μm^{-1}) and F the solar spectral irradiance at Jupiter (W cm^{-2} μm^{-1}). As stated earlier we used the solar spectrum of Chance and Kurucz (2010) for this, smoothed to the same resolution as the data. This spectrum, divided through by a Planck function of temperature 5778 K and normalised to 0.4 is also shown in Figs. 9 and 10 and there are several Fraunhofer absorption lines seen, the most prominent of which are highlighted. Any error in the assignment of wavelengths or instrument line shape would be most apparent in the reduced I/F spectra at the location of these lines, and we can see that, by and large, the I/F spectra are mostly smooth at the Fraunhofer line positions. Exceptions to this can be seen near ammonia absorption 'B' at 0.656 μm, where our reduction seems to overcompensate for the solar absorption line and to a lesser extent at the lines shortward of this. Elsewhere, the spectrum seems well modelled with our assumed methane absorption tables, based on the band data of Karkoschka and Tomasko (2010). Exceptions to this are at wavelengths between 0.656 and 0.7 μm, where although we fit the same peaks and troughs, the shape of the absorption features is not optimal. These discrepancies arise, we believe, from deficiencies in the methane band data at these wavelengths.

5. Conclusion

In this paper we have reviewed and assessed the reliability and consistency of different sources of ammonia absorption data when modelling the visible/near-infrared reflectance spectra of Jupiter from our VLT/MUSE observations. We have found that ammonia k-tables generated from the band models of Bowles et al. (2008) provide the best combination of reliability and wavelength coverage for the MUSE spectral range, although these data are found to be unreliable at wavelengths less than 0.758 μm. The data of Bowles et al. (2008) seem consistent with the ExoMOL ammonia line data of Yurchenko et al. (2011), where they overlap, but these latter data do not cover the ammonia absorption bands at 0.79 and 0.765 μm, which are prominent in our MUSE observations. At shorter wavelengths we find that the laboratory observations of Lutz and Owen (1980) provide a good indication of the position and shape of the ammonia absorptions near 0.552 μm and 0.648 μm, but their absorption strengths seem inconsistent with the available data at longer wavelengths and we have no reliable way to extrapolate the strength and shape of these bands to the cold, H_2-He broadening conditions in Jupiter's atmosphere. We also find that the line data of the 0.648-μm band of Giver et al. (1975) are not suitable for modelling these data as they account for only 17% of the band absorption and lack information on lower state energies, necessary to compute their absorption strengths at cold temperatures.

We conclude that in order to interpret such observations of Jupiter and Saturn more reliably in future there is a clear need to better define the absorption of ammonia gas at visible wavelengths. However, this need extends beyond our solar system. Space telescopes such as NASA's planned Wide Field Infrared Survey Telescope (WFIRST) (e.g. Spergel et al. 2013) have been proposed to detect and perform coronagraphic direct-imaging spectral observations of Jupiter-like planets about other stars. To interpret the spectra of such exoplanets requires that we have reliable absorption spectra of the absorbing gases,

of which ammonia is likely to be a key contributor. Hence, new estimates of the visible absorption spectrum of ammonia are crucial to extend our understanding of both solar system planetary physics and exoplanetary physics.

6. Acknowledgements

We are grateful to the United Kingdom Science and Technology Facilities Council for funding this research. The VLT/MUSE observations were performed at the European Southern Observatory (ESO), proposals: 095.C-0149, 096.C-0173, 098.C-0035 and 099.C-0192. We thank Larry Sromovsky for kindly providing the code we used to generate our Rayleigh-scattering opacities, Renyu Hu, for providing an electronic version of the line data of (Giver et al. 1975) and advising on the use of the linewidths of Keffer et al. (1985) and Keffer et al. (1986), and Sergi Hildebrandt and Margaret Turnbull (WFIRST Science Investigation Team PI) for coordinating the WFIRST Exoplanet Data Challenge, through which these discrepancies in ammonia absorption coefficients came to light.

Facilities: VLT (MUSE).

The k-tables used to generate the figures in this paper are available from the authors.

REFERENCES

Amundsen D. S., Baraffe I., Tremblin P., Manners J., Hayek W., Mayne N. J., Acreman D. M., 2014. Accuracy tests of radiation schemes used in hot Jupiter global circulation models. A&A, 564, A59.

Bacon, R., et al., 2010. The MUSE second-generation VLT instrument. Proc. SPIE 7735, Ground-based and Airborne Instrumentation for Astronomy III, 773508, doi:10.1117/12.856027.

Baines, K. H., Sromovsky, L. A., Carlson, R. W., Momary, T. W., Fry, P. M., 2016. The visual spectrum of Jupiter's Great Red Spot accurately modeled with aerosols produced by photolyzed ammonia reacting with acetylene. Icarus, 000, submitted.

Ballester, P, Banse, K., Castro, S., Hanuschik, R., Hook, R., Izzo, C., Jung, Y., Kaufer, A., Larsen, J., Licha, T., et al., 2006. Data reduction pipelines for the Very Large Telescope. in 'SPIE Astronomical Telescopes+ Instrumentation', International Society for Optics and Photonic, pp 62700T – 62700T.

Bowles, N., Calcutt, S., Irwin, P., Temple, J., 2008. Band parameters for self-broadened ammonia gas in the range 0.74 to 5.24 μm to support measurements of the atmosphere of the planet Jupiter. Icarus, 196, 612 – 624.

Carlson, R. W., Baines, K. H., Anderson, M. S., Filacchione, G., Simon, A. A., 2016. Chromophores from photolyzed ammonia reacting with acetylene: Application to Jupiter's Great Red Spot, Icarus, 274, 106 – 115.

Chance, K., Kurucz, R.L. 2010. An improved high-resolution solar reference spectrum for earth's atmosphere measurements in the ultraviolet, visible, and near infrared. J. Quant. Spec. Radiat. Transf., 111, 1289 – 1295.

460 Garland, R., Irwin, P.G.J., 2017. Effectively calculating gaseous absorption in radiative
461 transfer models of exoplanetary and brown dwarf atmospheres, MNRAS (submitted
462 and in review).

463 Giver, L.P., Miller, J.H., Boese, R.W., 1975. A laboratory atlas of the $5\nu_1$ NH_3 absorption
464 band at 6475Å with applications to Jupiter and Saturn. Icarus, 25, 34 – 48.

465 Goody, R.M., 1952. A statistical model for water-vapour absorption. Quart. J. R. Met. Soc.
466 78, 165.

467 Goody, R.M., Yung, Y.L., 1989. Atmospheric Radiation: Theoretical Basis (2nd Edition).
468 Oxford University Press, Oxford, UK.

469 Hansen, J.E., 1971. Multiple scattering of polarized light in planetary atmospheres. Part II.
470 Sunlight reflected from terrestrial water clouds. J. Atmos. Sci., 28, 1400 – 1426.

471 Irwin, P.G.J., Calcutt, S.B., Sihra, K., Taylor, F.W., Weir, A.L., Ballard, J., Johnston,
472 W.B., 1999. Band parameters and k-coefficients for self-broadened ammonia in the
473 range 4000 – 11000 cm^{-1}. J. Quant. Spec. Radiat. Transf., 62, 193 – 204.

474 Irwin, P.G.J., Parrish, P.D., Fouchet, T., Calcutt, S.B., Taylor, F.W., Simon-Miller, A.A.,
475 Nixon, C.A., 2004. Retrievals of jovian tropospheric phosphine from Cassini/CIRS.
476 Icarus, 172, 37 – 49.

477 Irwin, P.G.J., Teanby, N.A., de Kok, R., Fletcher, L.N., Howett, C.J.A., Tsang, C.C.C.,
478 Wilson, C.F., Calcutt, S.B., Nixon, C.A., Parrish, P.D., 2008. The NEMESIS plane-
479 tary atmosphere radiative transfer and retrieval tool. J. Quant. Spec. Radiat. Transf.,
480 109, 1136 – 1150.

481 Irwin, P.G.J., Tice, D.S., Fletcher, L.N., Barstow, J.K., Teanby, N.A., Orton, G.S., Davis,
482 G.R., 2015. Reanalysis of Uranus' cloud scattering properties from IRTF/SpeX

observations using a self-consistent scattering cloud retrieval scheme. Icarus, 250, 462 – 476.

Karkoschka, E., 1994. Spectrophotometry of the Jovian planets and Titan at 300 to 1000 nm wavelength: The methane spectrum. Icarus, 111, 174 - 192.

Karkoschka, E., Tomasko, M.G., 2010. Methane absorption coefficients for the jovian planets from laboratory, Huygens, and HST data. Icarus, 205, 674 – 694.

Keffer, C. E., Conner, C.P, Smith, W.H., 1985. Hydrogen broadening of vibrational-rotational transitions of ammonia lying near 6450Å. J. Quant. Spec. Radiat. Transf., 33, 193 – 196.

Keffer, C. E., Conner, C.P, Smith, W.H., 1986. Pressure broadening of ammonia lines in the 6475Å band at room and low temperatures. J. Quant. Spec. Radiat. Transf., 35, 487 – 493.

Lacis, A.A., Oinas, V., 1991. A description of the correlated-k distribution method for modelling nongray gaseous absorption, thermal emission, and multiple scattering in vertically inhomogeneous atmospheres. J. Geophys. Res., 96, 9027 – 9063.

Lutz, B.L., Owen, T., 1980. The visible bands of Ammonia: Band strengths, curves of growth, and the spatial distribution of Ammonia on Jupiter. ApJ, 235, 285 – 293.

Matousek, S., 2007. The Juno New Frontiers Mission. Acta Astronautica, 61, 932 – 939.

Nouri, S., Orphal J., Aroui H., Hartmann J.-M., 2004. Temperature dependence of pressure broadening of NH_3 perturbed by H_2 and N_2. J. Mol. Spec., 227, 60 – 66.

Pine, A., Markov V., Buffa G., Tarrini, O., 1993. N_2, O_2, H_2, Ar and He broadening in the ν_1 band of NH_3, J. Quant. Spec. Radiat. Transf., 50, 337 – 348.

505 Plass, G.N., Kattawar, G.W., Catchings, F.E., 1973. Matrix operator method of radiative
506 transfer. 1: Rayleigh scattering. Appl. Opt., 12, 314 – 329.

507 Rothman, L.S., Gordon, I.E., Babikov, Y., Barbe, A., Benner, D.C., Bernath, P.F., et
508 al, 2013. The HITRAN2012 molecular spectroscopic database, J. Quant. Spec. Ra-
509 diat. Transf., 130, 4 – 50.

510 Sharp, C. M., Burrows A., 2007. Atomic and molecular opacities for brown dwarf and giant
511 planet atmospheres, ApJS, 168, 140 – 166.

512 Sheik-Bahae, M., 2005. Nonlinear Optics Basics. Kramers-Kronig Relations in Nonlinear
513 Optics. In Robert D. Guenther. Encyclopedia of Modern Optics. Amsterdam:
514 Academic Press.

515 Spergel, D., et al., 2013. Wide-Field InfraRed Survey Telescope-Astrophysics Focused
516 Telescope Assets (WFIRST-AFTA) Science Definition Team (SDT) Final Report,
517 arXiv 1305.5422.

518 Sromovsky, L.A., Baines, K.H., Fry, P.M., Carlson, R.W., 2017. A possibly universal red
519 chromophore for modeling color variations on Jupiter, Icarus, 291, 232 – 244.

520 Thuillier, G., Hersé, M., Labs, D., Foujols, T., Peetermans, W., Gillotay, D., Simon, P.C.,
521 Mandel, H., 2003. The solar spectral irradiance from 200 to 2400 nm as measured by
522 the SOLSPEC spectrometer from the ATLAS and EURECA missions, Sol. Phys.,
523 214, 1 – 22.

524 Yurchenko, S.N., Barber, R.J., Tennyson, J., 2011. A variationally computed line list for
525 hot NH_3, MNRAS, 413, 1828 – 1834.

526 Zheng, C., Borysow, A., 1995. Modeling of collision-induced infrared absorption spectra of

H_2 pairs in the first overtone band at temperatures from 20 to 500 K. Icarus, 113, 84 – 90.

This manuscript was prepared with the AAS LaTeX macros v5.2.

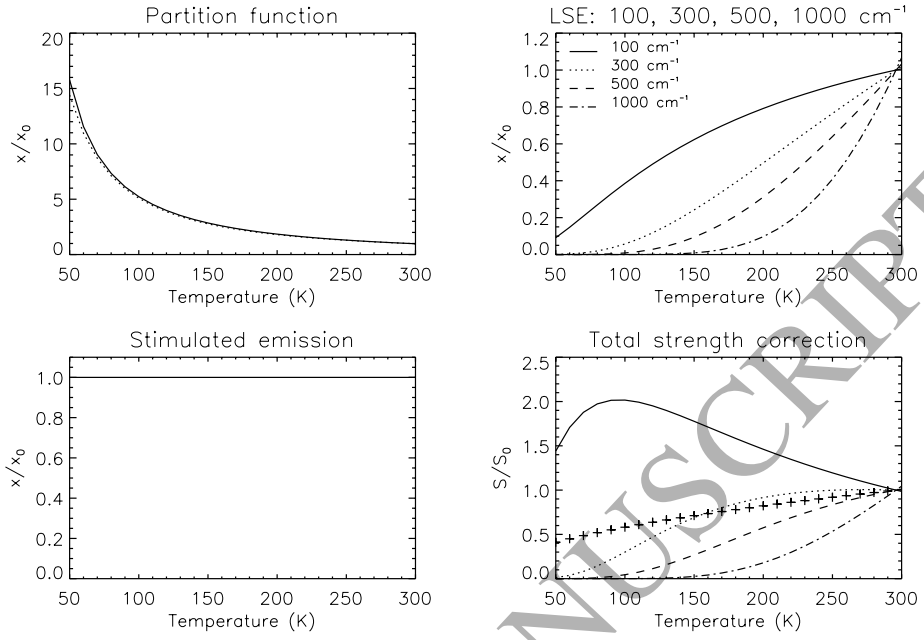

Fig. 1.— Temperature factors affecting line strength for ammonia lines near 6475Å. Top left panel shows the strength correction arising from the temperature dependance of the total partition function (computed using the HITRAN2012 temperature coefficients of Rothman et al. (2013)), which includes both the vibrational and rotational components. Overplotted (as a dotted line) is the expected rotational component alone, $(T_0/T)^{3/2}$, showing that this dominates at these temperatures. Top right panel shows the strength correction arising from the $\exp(-E_l/kT)$ term in Eq.1, for lower state energies, E_l, of 100, 300, 500 and 1000 cm^{-1}, indicated by the different line styles defined in the panel. Bottom left panel shows the correction arising from the temperature dependence of the stimulated emission term, which is clearly negligible at these temperatures and wavelengths. Bottom right panel shows the combined effects of all these factors on the line strength, with again the factors for different lower state energies indicated by the different line styles defined in the top right panel. Also shown, for comparison, is the dependance of the band-integrated absorption assumed by Lutz and Owen (1980) for their laboratory observations at 5520 and 6475Å, i.e. $S = S_0(T/T_0)^{1/2}$, marked with the 'plus' symbols.

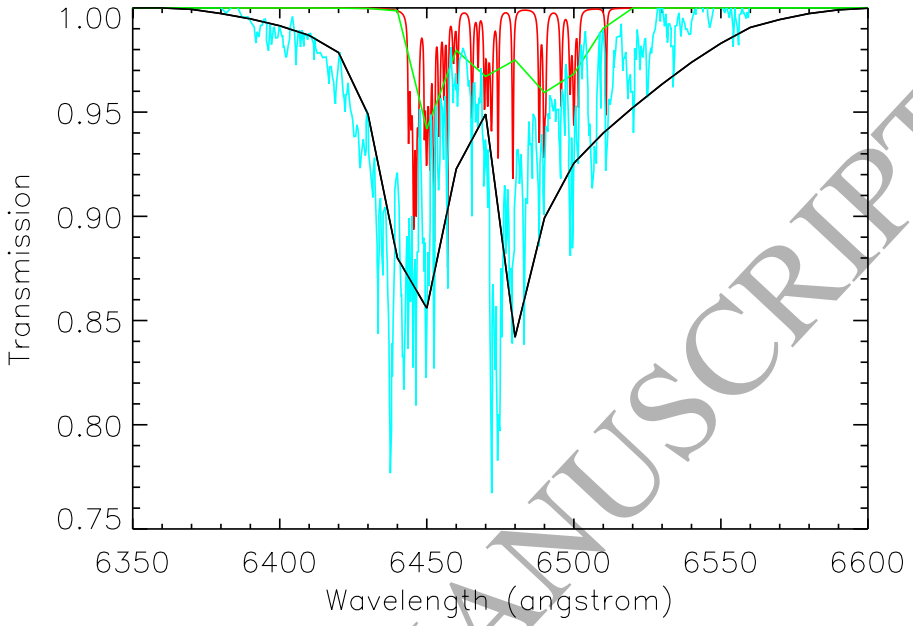

Fig. 2.— Transmission spectrum of the self-broadened path of ammonia shown in Fig.3 of Giver et al. (1975). In this calculation the temperature is 294 K, the path length is 36 m and the pressure is 1 atm. The originally measured 'low-dispersion' spectrum of Giver et al. (1975) (digitised by the authors) is shown, coloured in cyan, while the red line shows a high resolution spectrum calculated using the line data of Giver et al. (1975) described in this paper (using the self-broadened widths quoted by Giver et al. (1975)). The black line shows the spectrum calculated with the absorption coefficients of Lutz and Owen (1980) that have a resolution of 2Å (or 0.0002 μm), which shows much better agreement with the measured transmission spectrum, albeit at lower resolution. The green line shows the spectrum calculated from the Giver et al. (1975) line data smoothed to a resolution of 2Å to allow direct comparison with the absorption coefficients of Lutz and Owen (1980). It can be seen that the line data do not cover the complete range and do not account for enough of the weaker lines to be able to fully account for the observed band absorption.

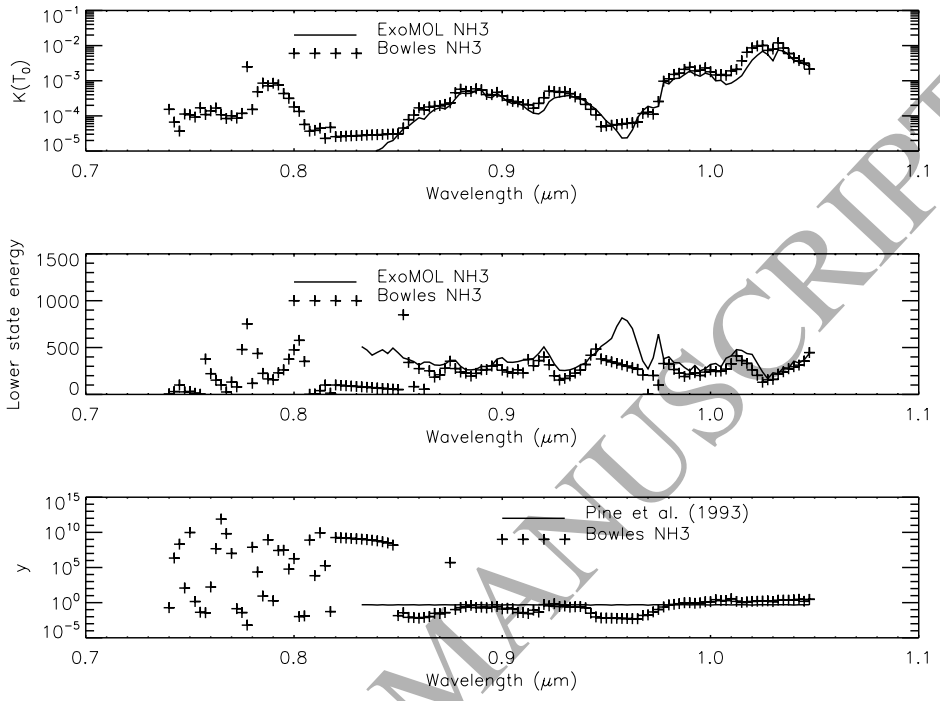

Fig. 3.— Comparison of NH_3 band parameters ($k_\nu(T_0)$, E_l and y_ν) of Bowles et al. (2008) with the equivalent parameters extracted from the ExoMOL line data (Yurchenko et al. 2011), averaged into the bins used by Bowles et al. (2008), which have a step and FWHM of 0.0025 μm between 0.74 and 1.0475 μm. The absorption coefficients, $k_\nu(T_0)$, (top panel) are in units of (molecule cm^{-2})$\times 10^{24}$. These are directly extracted from the data of Bowles et al. (2008) and shown as the cross symbols. For the ExoMOL data, these absorption coefficients are the average line strength (at T_0) across the bins, shown as the solid line. The middle panel shows the lower state energies E_l, quoted by Bowles et al. (2008), together with the bin-averaged and strength-weighted lower state energies for ExoMOL. Finally, the bottom panel compares the y_ν parameter of Bowles et al. (2008), with the bin-averaged, strength-weighted self-broadened line widths of Pine et al. (1993).

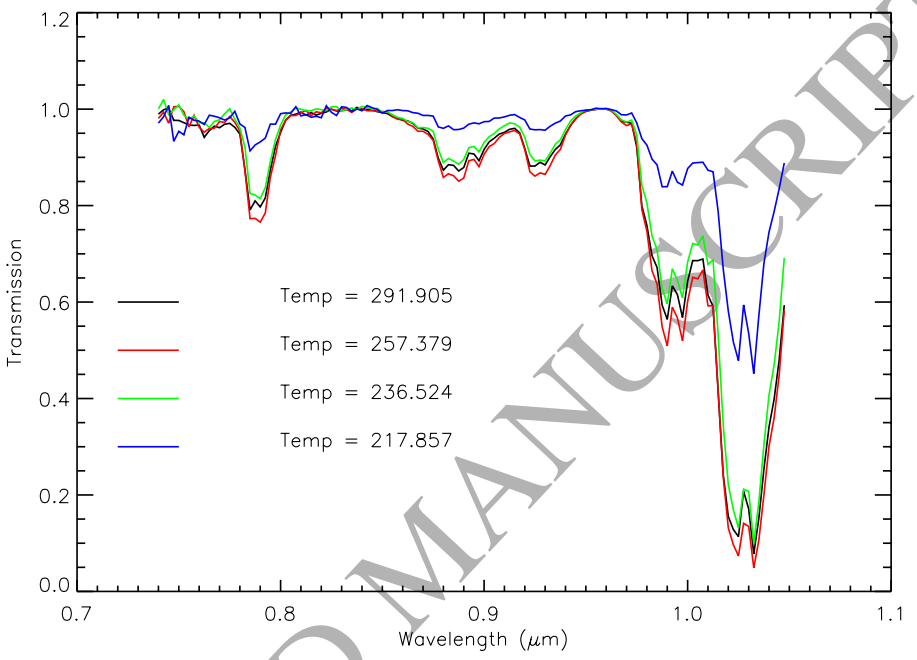

Fig. 4.— Longest path absorber amount, U, (i.e. molecule cm^{-2}) laboratory-measured self-broadened transmission spectra of Bowles et al. (2008) for temperatures in the range 200 – 225 K, 225 – 250 K, 250 – 270 K, and 280 – 300 K. The actual temperatures are listed in the figure, while the corresponding pressures are 223, 707, 1022 and 1027 mb respectively. All transmission spectra were measured for the longest path length of 10.164 m. We can see that the laboratory data seem to be consistent for wavelengths longer than $\sim 0.76\mu$m, but vary inconsistently with temperature at lower wavelengths and seem to be dominated by noise.

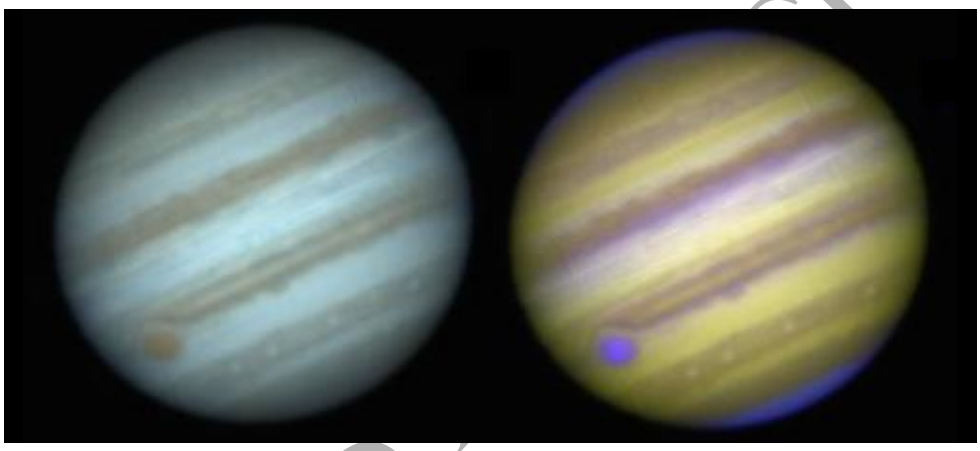

Fig. 5.— Left: 'True Colour' composite MUSE image constructed from data recorded on March 8th 2016 (02:49:38UT). The GRS is clearly visible at lower left. Right: False-colour image, where red is reflection at 630 nm (weak methane absorption), green is reflection at 510 nm (sensitive to blue-absorbing 'chromophores'), and blue is reflection at 890nm (strong methane absorption, sensitive only to high level hazes).

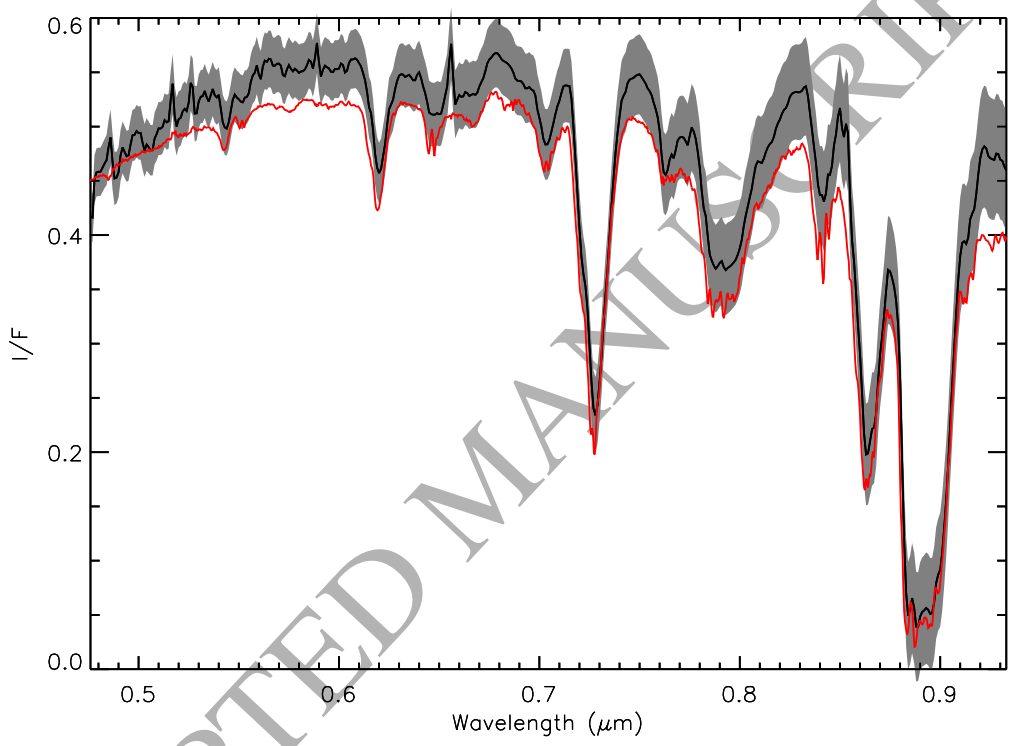

Fig. 6.— Disc-averaged MUSE spectrum (and variance) shown in grey, observed on 28th May 2017 at 01:31:25UT. The red line shows the disc-averaged albedo spectrum of Jupiter measured in 1993 (Karkoschka 1994) for comparison, showing good correspondence even after an elapsed time of 24 years.

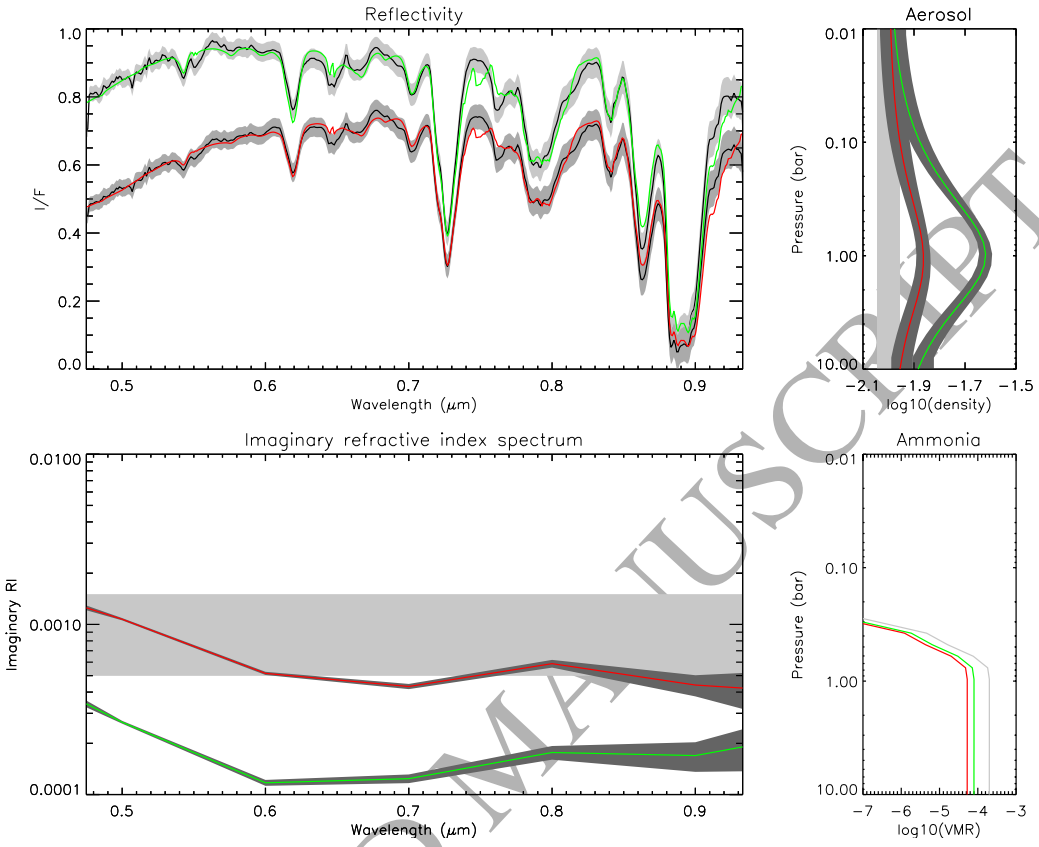

Fig. 7.— Fit to representative Equatorial Zone (EZ) and North Equatorial Belt (NEB) spectra observed on 28th May 2017 at 01:31:25UT with VLT/MUSE. Top left panel shows our fit to spectra averaged over the central portion of the Equatorial Zone (EZ) and North Equatorial Belt (NEB), as described in the text, with estimated error range (including forward model errors) shown in grey. The fits to these spectra using our NEMESIS retrieval model are shown in green (EZ) and red (NEB). Top right panel shows the fitted cloud density profiles (in units of opacity/(g cm^{-2}) at 0.6 μm) retrieved at these locations for the EZ(green) and NEB(red), with fitted error ranges in dark grey and *a priori* error range in light grey. Bottom right panel shows the *a priori* assumed ammonia profile (grey), together with the fitted scaled profiles in the EZ(green) and NEB(red). Finally, the bottom left panel shows the fitted imaginary refractive index spectra of the cloud particles in the EZ(green) and NEB(red), with fitted errors again shown in dark grey and *a priori* assumed values in light grey.

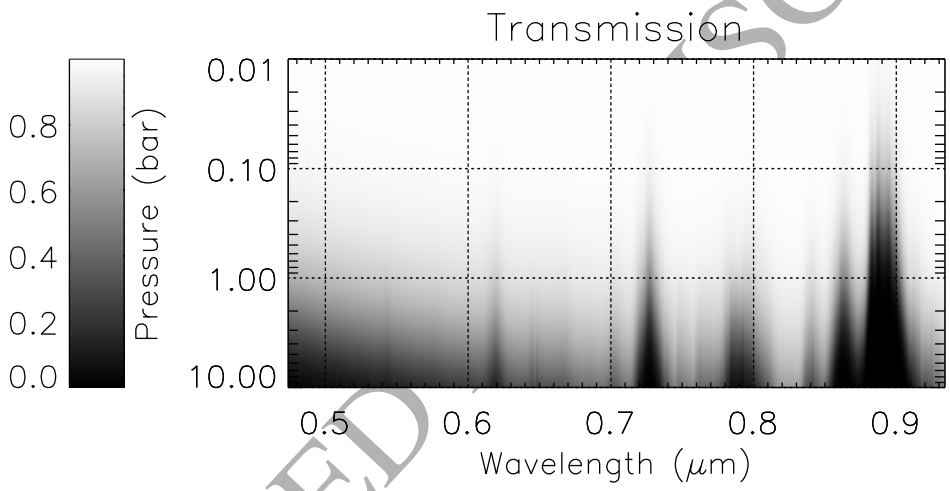

Fig. 8.— Two-way transmission calculated to different levels in Jupiter's atmosphere for a vertical path in cloud-free conditions.

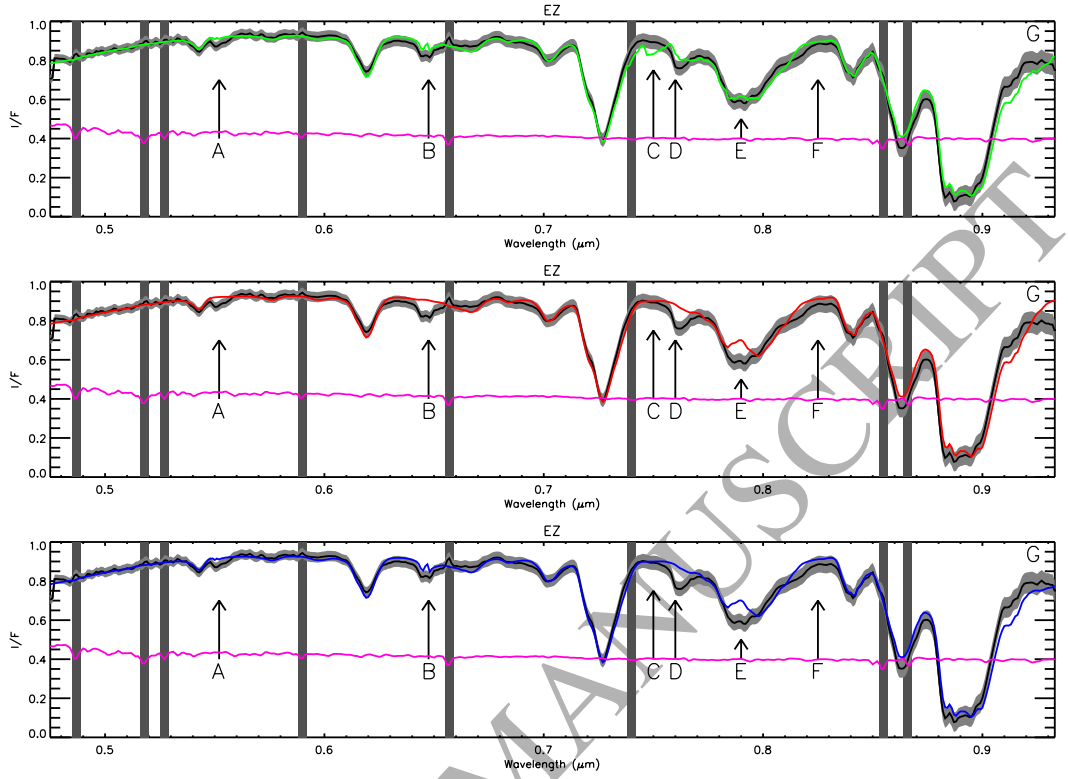

Fig. 9.— Observed MUSE spectrum averaged over the central portion of the Equatorial Zone (EZ) with estimated error (including forward model errors) shown in grey, observed on 28th May 2017 at 01:31:25UT. In the top panel, the green line is the fit of our NEMESIS retrieval model using the ammonia absorption data of Bowles et al. (2008) and Lutz and Owen (1980). In the middle panel, the observed spectrum is compared with the calculated spectrum when the ammonia absorption data of Bowles et al. (2008) and Lutz and Owen (1980) are neglected, shown in red. In the bottom panel, the observed spectrum is compared with the calculated spectrum when the absorption of ammonia at wavelengths $> 0.7\mu$m is modelled instead with ExoMOL (Yurchenko et al. 2011), shown in blue. The labelled features 'A' to 'G' mark the main observable ammonia absorption features, which are discussed further in the text. Also shown in purple is the assumed solar spectrum of Chance and Kurucz (2010), divided by a Planck function of temperature 5778 K and scaled to give a value of ~ 0.4, showing the various Fraunhofer lines in the spectrum. The most significant of these are highlighted by the darker grey bars. As we divide the measured radiance spectrum by this solar spectrum, any error in line width or position can potentially lead to errors at the Fraunhofer wavelengths.

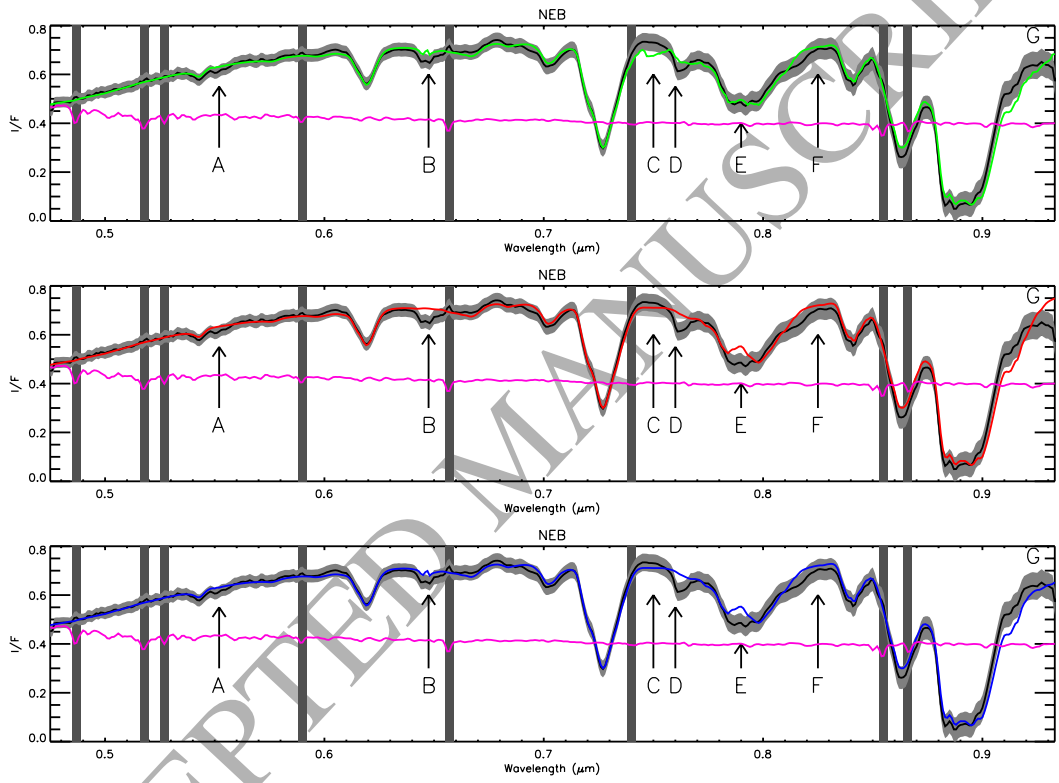

Fig. 10.— As Fig.9, but comparing our calculations for different ammonia absorption sources with the observed MUSE spectrum averaged over the North Equatorial Belt (NEB).